Modelling the aerodynamic response of a wind turbine blade passing in front of the tower

Modelling the aerodynamic response of a wind turbine blade passing in front of the tower

Wolf-Gerrit Früh[1], Jörg Seume[2], Alejandro Gomez[2]
[1] School of Engineering and Physical Sciences,
Heriot Watt University, Riccarton, Edinburgh EH14 4AS, UK
[2] Institute for Turbomachinery and Fluid Dynamics,
University of Hannover, Appelstr. 9, 30167 Hannover, Germany
email: w.g.fruh@hw.ac.uk

March 27, 2008

Abstract

It is recognised that even upwind turbines feel the presence of the supporting tower in a pulse of the output known as 3p oscillations. Here we investigate the aerodynamics of this phenomenon by modelling the upwind perturbation of the free wind through the tower as a time-dependent boundary condition on a Computational Fluid Dynamics (CFD) model of a turbine blade section.

To model the origin of the 3p oscillation, the perturbation of the free wind upstream of a cylindrical tower is modelled as the ideal flow solution of the flow around a cylinder. In the second step of the analysis, the local relative velocity field around a turbine blade section is found as a function of the free wind, the tower dimensions, the blade overhang, and the time-dependent position of the section in that flow as the blade rotates around the hub. The resulting velocities and pressure variations are then used as time dependent boundary conditions of a 2D-CFD model using the software package NUMECA based on the S809 aerofoil section. Two basic turbulence models were tested, the one-equation Spalart-Allmaras model and the two-equation k-ω model.

The analysis of the perturbation flow field shows that the tower shadow not only causes a short pulse of the effective velocity but also an even sharper change of the effective angle of attack of around 10%. The results suggest that the overall effect is a moderate reduction of the time-averaged torque coefficient compared to the simple flow over the aerofoil section. Over the range of wind speeds investigated, the magnitude of this effect appears to be largely unaffected by the distance between the blade and the tower. However, at high effective angles of attack, the results indicate that the onset of stall is delayed if the distance between the blade and the tower is stall. It appears that the increasing pulse caused by the passing in front of the tower acts as a mechanism to re-attach the flow which would be fully detached in the free case.

1 Introduction

As utility-sized turbines are becoming increasingly larger, the forces on the structures are also increasing substantially. Of particular concern to the performance of a turbine and its reliability are variations in the forces on the turbine blades, the nacelle, and the towers. One particular phenomenon is known as the 3p-effect, named after the observation of a flicker in the electical output at a frequency of three times the rotation rate of the rotor from the most common type of utility-sized turbines, namely three-bladed horizontal axis wind turbines, e.g. [9, 3].

While the basic aerodynamics of wind turbines is well understood – and well exploited with current efficiencies of 50% compared to the theoretical limit of 59% – other 'smaller' effects may have strong effects on a wind turbine's operation[5]. One of these is 'dynamic stall' where the turbine blade loses productive torque at some orientation of its rotation and fails to recover lift even though the wind

conditions at other orientations of the blade should result in productive forces [4]. It is suggested that dynamic stall results from the inability of a separated boundary layer to re-attach.

A systematic parametric study of the flow conditions for wind turbines, summarised in section 2, shows that the flow over a wind turbine blade would either be fully turbulent *ab initio*, due to the free-stream turbulence intensity in the atmospheric boundary layer, or that the transition would occur in most cases within the first 10% of the blade surface. It was found furthermore, that the rotor would experience a time-dependent variation in the inflow conditions not only due to the vertical variation of the wind speed, known as the 'wind shear' but that it would also feel a short but noticeable pulse due to the modification of the wind as the air approaches the turbine tower. As a result, we report here an investigation of the response of fully turbulent flow over a typical aerofoil section subject to time-dependent boundary conditions mimicking both, wind shear and tower shadow.

The next section presents the analysis of the inflow conditions subject to wind shear and tower shadow. The following section, § 3, then introduces the aerofoil and boundary geometries investigated, the numerical model to simulate the system, and the computational methodology. Section 4 describes the numerical results before the final section which contains the Conclusions.

2 Parametric study of realistic flow conditions

As the rotor blade swepts around, the local wind conditions change and lead to the onset of stall followed by a return to conditions which should not lead to stall. Yet, the flow does not have the time get out of stall conditions and the flow around the blade remains stalled, with loss of productive torque and increase in axial loading. Two factors have been identified and are discussed below. One of these is that the wind increases with height from the ground and the other is due to a modification of the wind due to the turbine tower even when the tower is behind the rotor.

2.1 Typical Reynolds number range

In this section, typical operating conditions are presented for two representative turbines, the small 10m turbine of the NREL experiment [8, 7], rotating at 78rpm, and the Vestas V80-2MW. The Vestas is a typical modern wind turbine with a rotor diameter of 80m and a rated output of 2MW. Its turbine blades have a chord length of about 3m at the root which tapers down to about 1m near the tip. At the cut-in wind speed of 4m/s it rotates at 9rpm, then increases the rotation rate linearly up to 16.7rpm at wind speed of 8m/s, above which it remains constant. Using these data, one can determine the Reynolds numbers for the average flow over the turbine blades which varies along the blade from the hub to the tip. As the distance from the hub increases, the relative fluid velocity increases but the chord length decreases. The overall balance for the two turbines, in figure 1, shows that the Reynolds number for the small turbine is between 10^5 and 1.5×10^6, while that for the large turbine is always greater than 10^6. This demonstrates that a small turbine may be affected by the transition to turbulence at slow to moderate wind speeds but that the flow over a large wind turbine will almost certainly be turbulent for most of the blade chord over the vast majority of positions along the blade even at small wind speeds.

2.2 Wind shear

As a turbine blade moves, it finds itself at times nearer the ground where the wind speed is slower and at other times higher up where the wind is higher. This variation of the velocity in the turbulent planetary boundary layer with height is known as wind shear. Two types of profiles are commonly used to approximate the increase of the wind with height, a logarithmic and a power-law curve, e.g. [6, 2]. The logarithmic profile can be applied to a neutral or unstable atmosphere,

$$U(z) = U_0 \ln(z/z_r)/\ln(z_0/z_r), \tag{1}$$

where z_0 is a reference height and z_r is a surface roughness. The surface roughness depends on the topography, ranging from $z_r = 2 \times 10^{-4}\mathrm{m}$ for the open sea, through $0.03\mathrm{m}$ for open flat terrain to

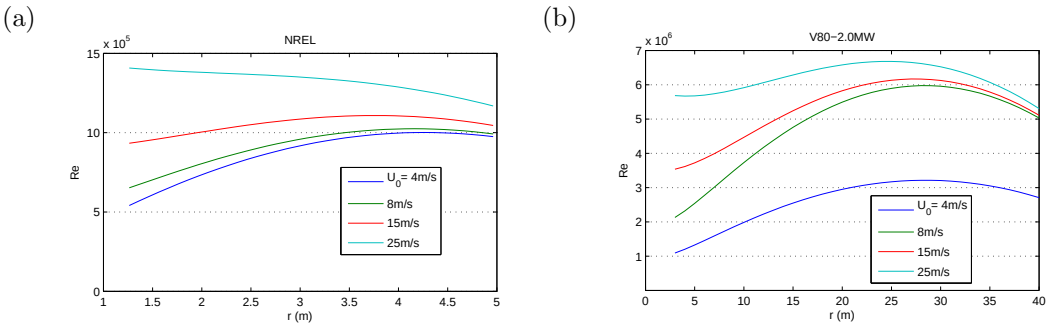

Figure 1: The Reynolds number of the flow over a wind turbine blade against the position along the blade for a number of wind speeds from the cut-in speed of 4m/s to the cut-out speed of 25m/s: (a) for the NREL 10m turbine, (b) for the Vestas V80-2MW turbine.

$0.5 - 1\mathrm{m}$ for a forest or suburb. The other profile does not take the surface roughness into account but can be applied to both, stable and unstable conditions. Its form is

$$U(z) = U_0(z/z_0)^m, \tag{2}$$

where m characterises different atmospheric conditions from $m = 0.09$ for a very unstable atmosphere, through $m = 0.22$ for a neutral atmosphere, to $m = 0.41$ for very stable conditions. Wind profiles for a wind speed of 8m/s at a reference height of 10m are shown in figure 2 for all extreme cases of wind shear profiles.

Under stable, conditions which tend to be associated with lower wind speeds, the variation for the 2MW turbine on a mast of between 60m and 100m may change by up to about 30%. At a wind speed of 4m/s at 10m height, this would result in a range of Reynolds number from about 3.5×10^6 at a height of 20m to about 5×10^6 at a height of 100m. Under unstable or offshore conditions, the wind speed varies by about 10% across the rotor.

2.3 Tower shadow

It is well known that downwind turbines, with the rotor behind the tower, experience significant forces due to the tower shadow. However, even upstream of the tower is the wind affected by the presence of the tower. Assuming that the flow upstream of the tower is close to ideal flow, the upstream effect of the tower on the flow at positions x and y from the tower centre can be estimated from the potential flow solution around a cylinder section of radius R_0:

$$u_x = U_0\left[1 - \left(R_0^2/r^4\right)\left(x^2 - y^2\right)\right] \tag{3}$$

and

$$v_y = -2U_0 xy R_0^2/r^4 \tag{4}$$

with $r^2 = x^2 + y^2$. As a result, the stream-wise component of the wind is reduced by 2% at 7.6 tower radii (R_T), 11% at $3R_T$, and 25% at $2R_T$. However, the lateral velocity induced by the tower has a stronger effect, as it modifies the effective velocity in the rotational direction of the rotor and therefore the effective angle of attack. This is illustrated in figure 2(b) for a wind speed of 15m/s, a blade velocity of 50/s, and an angle of attack of 11.7° if the wind shear is neglected. As the blade moves in front of the tower, the effective angle of attack increases at first as the air is deflected towards the incoming blade, but then the angle of attack drops suddenly by almost 1° as the x-velocity is reduced and the y-velocity is deflected the other way.

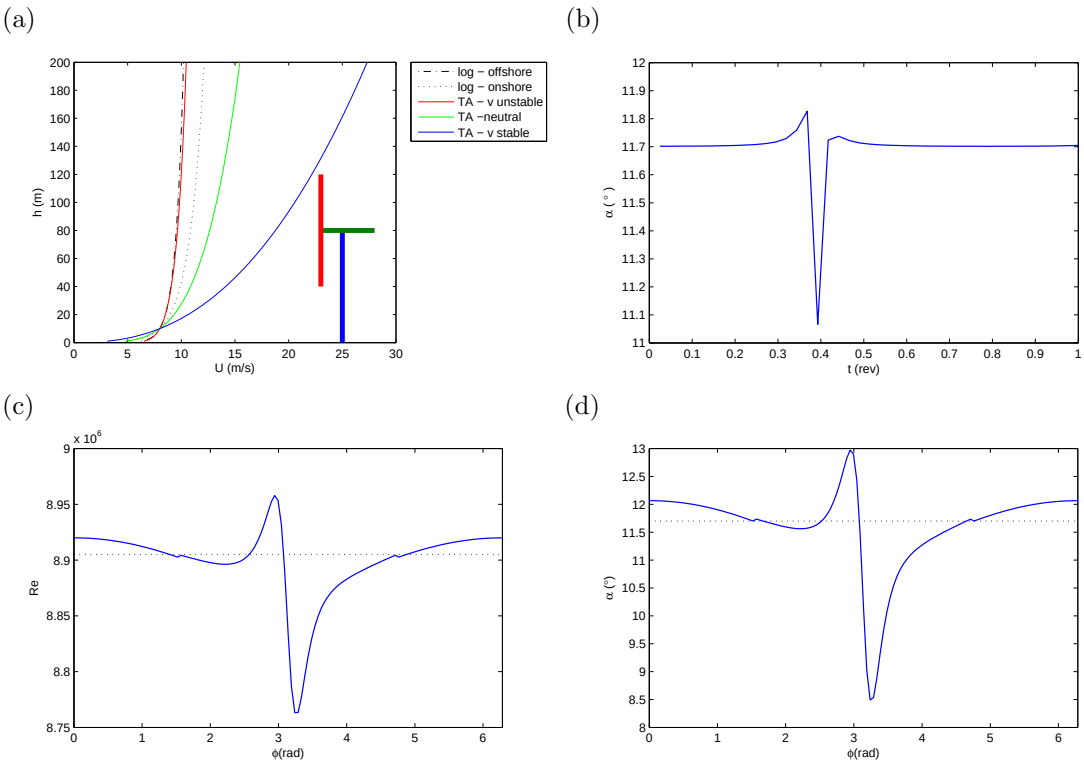

Figure 2: (a) Wind profiles for a wind speed of 8m/s at a reference height of 10m. A Vestas V80 on an 80m tower is shown for reference. (b) Variation of the effective angle of attack due to passing in front of the tower for a typical case of a wind speed of 15m/s and a blade velocity of 50m/s. (c) Combined effect of wind shear and tower on the Reynolds number. (d) Combined effect of wind shear and tower on the effective angle of attack.

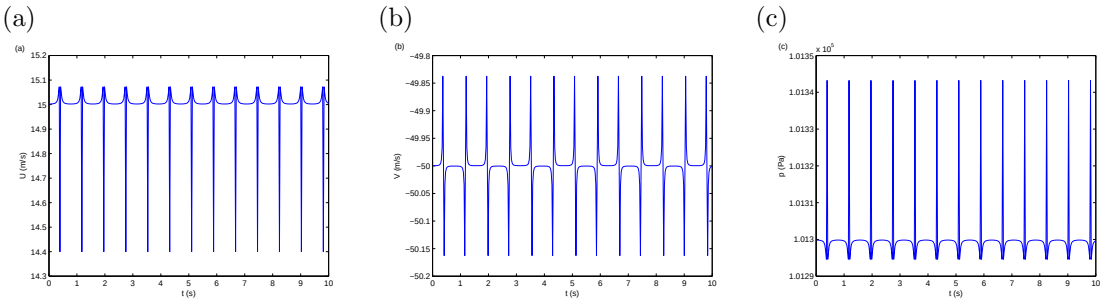

Figure 3: Time series of the boundary conditions for time-dependent forcing, (a) x-velocity of the wind, (b) y-velocity of the blade motion, and (c) pressure.

2.4 Summary

The effect on the Reynolds number and the effective angle of attack of the combination of rotational sampling of wind shear and the presence of the tower is illustrated in figures 2 (c) and (d) respectively. The variation of the Reynolds number is small (2%) but the variation of the effective angle of attack is substantial in this case (almost 40%), where most of the variation is due to the blade passing in front of the tower.

3 Model description and Methodology

3.1 Geometries

The system investigated here simulated the passing of an aerofoil section on a circular orbit some distance upstream of a circular tower, where the centre of the orbit is at the top of the tower. The blade section used had an aerofoil S809 cross-section for the reason that this is the profile of the NREL turbine blades, for which detailed measurements and computational results exist. For the model, a chord length of $c = 1\mathrm{m}$ was chosen for reference, and the angle of the chord line to the wind was $85°$. The tower had a diameter equal to the chord length and was positioned c, $1.5c$, or $2c$ downwind of the blade, respectively.

The wind conditions, $\mathbf{u}_w = (u_w, v_w, 0)$, are the mean horizontal flow induced by a mean wind, U_0, at the tower height modified by a wind shear of a typical onshore logarithmic profile and, at blade positions below the top of the tower, modified by the ideal flow induced by the tower. The local pressure was the gauge pressure calculated from Bernoulli's equation. The blade velocity, $\mathbf{u}_b = (0, v_b.w_b)$, is given by the section a distance along the blade which rotates around the shaft at the rotation rate of the NREL turbine of 78rpm. The magnitude of the blade speed was chosen as a reference speed of either $|U_b| = 50\mathrm{m/s}$ or 100m/s while the mean wind U_0 was varied from 5 to 80m/s. The boundary conditions imposed on the numerical model were then the relative velocity and pressure of the blade to the wind. An example of those boundary conditions for the two velocity components and the pressure are shown in figure 3, where the rotation rate of 78rpm is reflected in the period of the perturbation of 0.77s or 13 revolutions in the 10s interval shown.

3.2 Numerical model

The aerofoil geometry was created for use in the commercial CFD package *Numeca* which is specifically designed for aerodynamic studies in rotating machinery, both for internal flows such as gas turbines and external flows such as wind turbines. Various types of mesh topologies, including a C-grid and a combination of H grids, at different resolutions were tested with very little difference between the solutions. The final mesh used in the integrations presented below consisted of an O-grid surrounding the aerofoil embedded in two H-grids to include the further surrounding of the rotor, shown in figure 4. For all integrations, it was ensured that the CFL criterion was satisfied. In some cases, tests were

(a) (b)

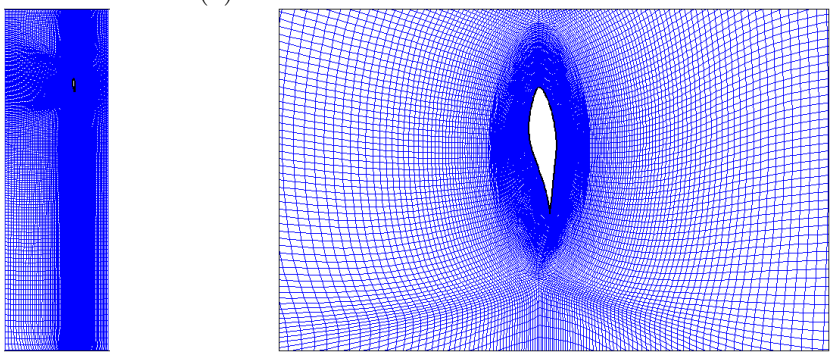

Figure 4: The full domain and a close-up of the model using the O-grid embedded in two H-grids

carried out for a range of the Courant number, from 3 down to 0.01. These showed consistent and virtually identical results for all cases where the Courant number was less than 1.

3.3 Methodology

The model geometry used for all integrations was the aerofoil with an angle between the wind and its chord line of 85°. For all mesh types and different turbulence models, the approach was to create a set of solutions for steady forcing, that is the flow over the aerofoil without wind shear or tower shadow. This was created from a first solution at low wind speed which was initiated first with a steady-state solver to a first approximation of the solution from which an equilibriated time-dependent solution was found by integrating over 10 or 20s. The final time-step was then used as the intial condition for a run at a slightly higher wind speed, and so on. A visual inspection of all time series showed that the solution had converged to an equilibrium during the first 4 to 5s of the run. For the analysis of the time-varying quantities and their time-average, only the second half of each time series was used. Some integrations were extended by a further 10s to confirm that the solution had reached an equilibrium.

Once a complete set of steady-forcing was obtained, those solutions were taken as the initial conditions for model integrations with the time-dependent boundary conditions simulating the wind shear and tower shadow.

4 Results

4.1 Choice of turbulence model

The intial C-grid was used to investigate the flow under steady inflow conditions for a range of wind speeds and and angles of attack. For a representative case (wind speed $U_0 = 30\mathrm{m/s}$, resulting in an angle of attack $\alpha = 11.7°$ – compared to a known measured angle of attack of $\sim 15°$ for onset of static stall), a number of turbulence models were tested, from the one-equation Bladwin-Lomax and Spalart-Allmaras models to a number of variants of two-equation *k*-ε (with and without extended wall function) and *k*-ω *Wilcox* and *SST* models. The results from the various *k*-ε models were all similar to each other but not consistent with measurements reported in the literature; they showed a boundary layer detaching well before it would be reasonably expected. This supported the common observations that this type of turbulence model does not perform particularly well for external flow with a detaching boundary layer. The Spalart-Allmaras model, on the other hand, showed fully attached flow while the *k*-ω *SST* model showed a separation bubble near the trailing edge of the aerofoil. The pressure distribution around the aerofoil for these two cases and the *k*-ε model with extended wall function are shown in figure 5, clearly showing fully attached flow in (a) for the Spalart-Allmaras model, a small separation bubble for $y > 0.8$ for the *k*-ω *SST* model in (b), and separated flow from $y >\sim 0.4$ for the *k*-ϵ model in (c). As the angle of attack investigated is in a region where the measured lift

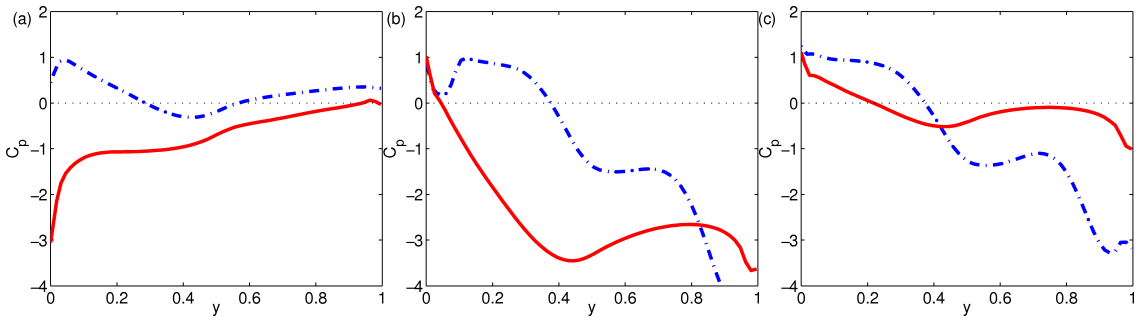

Figure 5: Comparison of standard turbulence models. Distribution of the pressure coefficient, $C_p = p/(\frac{1}{2}\rho U^2)$, around aerofoil for wind speed $U_0 = 15\mathrm{m/s}$, blade speed $V_b = 50\mathrm{m/s}$, angle of attack $\alpha = 11.7°$. (a) Spalart-Allmaras model, (b) *k-ω SST* model, and (c) *k-ε* model with extended wall function.

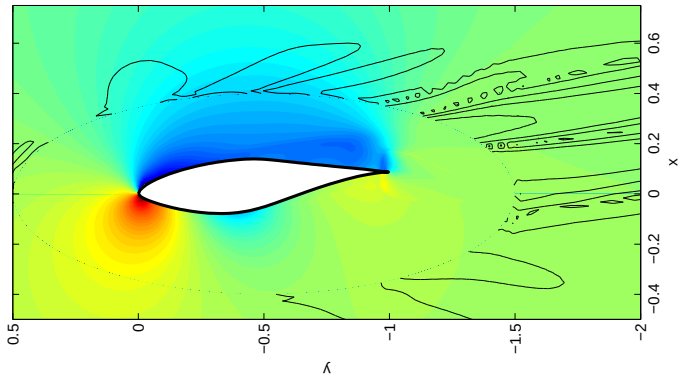

Figure 6: Snapshot of the pressure field and some vorticity contour lines around the aerofoil for a typical with time-varying forcing.

coefficient is near the optimum lift, it was decided to cover a range of angle of attacks with both, the Spalart-Allmaras and the *k-ω SST* model. The Spalart-Allmaras model delayed the onset of stall to an angle of attack of about $20°$, while the *k-ω SST* model showed full stall conditions at an angle of attack of $13°$. For the integrations described in §4.2, the *k-ω SST* model was used.

4.2 Effect of wind speed and tower distance

Figure 6 shows an example of the last time step of a time-dependent forcing with the pressure field and some vorticity contours. The vorticity contours indicate a substantial contribution of temporal fluctuations maintained by the temporal variation of the forcing. The pressure field shows that the pressure on the suction side (the upper surface) increases at this instant towards the middle of the aerofoil and then decreases again. This is actually the result of the separation of the low-pressure boundary layer, its advection downstream, and its re-attachment near the trailing edge.

Figures 7 and 8 show two illustrations of the effect of the wind shear and tower shadow. The temporal response of the flow to the time-varying forcing is demonstrated by comparing a time series of the torque coefficient for the steady forcing and a time-dependent forcing of otherwise identical conditions, shown in figure 9 (a) and (b), The torque coefficient is the nondimensionalised force in the y-direction, which applies the torque to turn the rotor against the power take-off. The force components in the x and y directions are quantities computed and provided by *Numeca* from the invisicid part (the

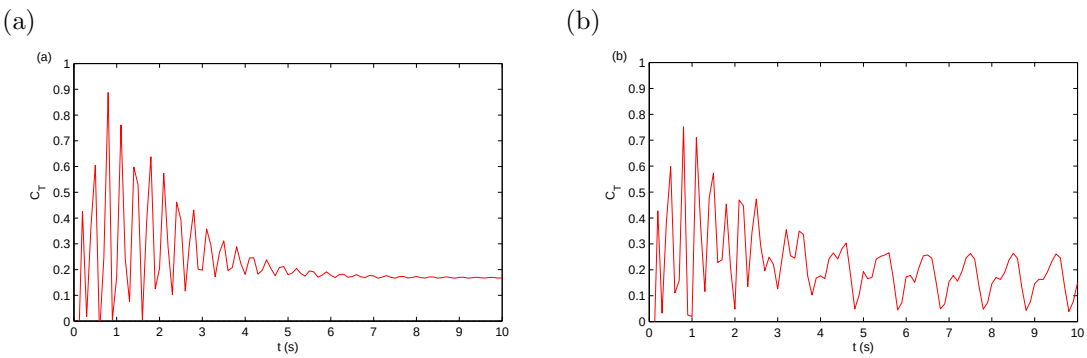

Figure 7: (a) Time series of the torque coefficient for a case with steady forcing (wind speed 5m/s, blade velocity 50m/s, effective angle of attack 2°) (b) time series of the torque coefficient with time-dependent forcing mimicking a tower with a spacing between the blade and the centre of the tower of $2c$, otherwise same conditions as in (a).

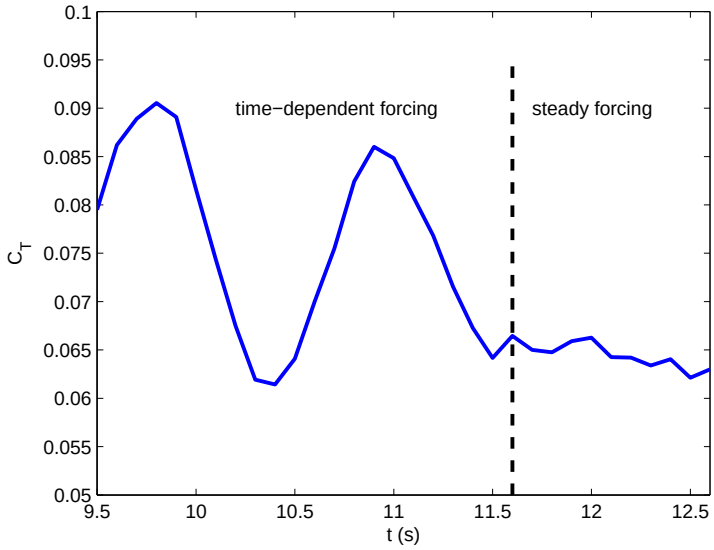

Figure 8: Time series of the calculated torque coefficient, first with the tower shadow effect and then, continued with constant boundary conditions. Wind speed 23m/s, blade velocity 100m/s; tower to blade distance: $1.5c$.

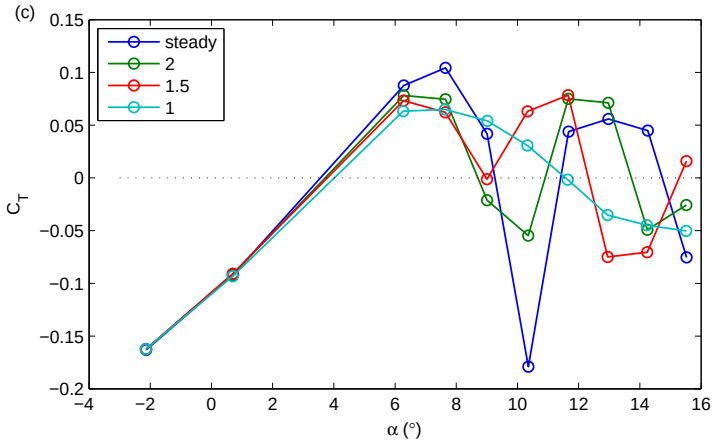

Figure 9: Variation of the time-averaged torque coefficient against the effective angle of attack for steady forcing and three distances between the blade and tower.

pressure distribution) and the viscous force (the shear force on the boundary).

Figure 7(a) shows the equilibration of the flow as the torque coefficient against time under steady forcing from the initial settling period to the equilibrated flow at around 5s. This flow is then continued but under time-dependent boundary conditions. After an intial transient, it can be seen in Figure 7(b) that the solution responds at the time scale of the rotation rate of the turbine. However, the response is not an immediate response since the abrupt loss of torque, e.g. just before 5 or 10s is not aligned with the sharp pulse of the forcing but precedes it by a noticeable fraction of the rotation period. It is more the shoulder during the phase of increasing torque which co-incides with the pulse from passing the tower. A visual inspection of the two figures shows that the maximum torque of the time-dependent case exceeds that of the steady forcing but that the time-averaged torque coefficient of the time-dependent forcing is less than that of the case with steady forcing. In one case, and extended simulation was performed, where the time-dependent forcing was maintained for 15 revolutions of the blade, followed another period by constant forcing. The break in the type of forcing is clearly reflected in the applied torque which becomes almost steady as soon as the time-dependent forcing is switched off.

Behaviour consistent with these examples is found at other flow conditions, as is demonstrated by the averaging of the torque coefficient over the equilibrated part of the time series and plotting it against the mean effective angle of attack of the different integrations, shown in figure 9. The magnitude of the temporal variation of the forcing, as given by the distance between the blade and the tower does not seem to play a major role for the mean torque, as the comparison of the three lines for the 'largely attached' part of figure 9 shows. All three are below the steady curve, initially such that the curve with the strongest tower shadow is lowest. Near maximum torque, and close to onset of stall, however, the case with the blade closest to the tower begins to have a larger time-averaged torque coefficient than the other two cases with tower shadow. Continuing those lines into the deep stall region, shows that the loss of torque is much less for the case where the tower is closest to the blade.

5 Conclusions

Following a short survey to explore the relative magnitude of the effect of wind shear and tower shadow in unsteady aerodynamics of wind turbines, we have used those results to develop a simple, yet high-resolution model of this situation with the aim to carry out a systematic parametric analysis of the flow response to those effects. As was expected from common experience in CFD application, the results depend strongly on a judicial choice of turbulence closure model. A comprehensive comparison

of commonly available turbulence models confirmed both, that flow separation would likely play a significant role in the our case and that $k-\epsilon$-type models are not appropriate to describe flow separation. Two candidates presenting 'reasonable' results were the one-equation Spalart-Allmaras model and the $k-\omega$ SST model, though again, the two turbulence model types showed strong, systematic differences in their prediction of flow separation. Without having measurements available, it is impossible to know which is the most appropriate turbulence model for any specific application. With increasing computational power, it is likely that LES or DES models will become the norm for modelling of turbulent flows.

An analysis of the pressure distribution over the aerofoil surface at different flow conditions suggests that the response of the blade to tower shadow, and the phenomenon of dynamic stall, are based in the separation of the boundary layer under stall conditions followed either by the inability of the separated flow to re-attach to the boundary or by re-attachment which is aided by the short pressure and velocity pulse resulting from the blade passing in front of the tower. It appears that the sharp spike, especially in the effective angle of attack, provides a mechanism to re-attache the boundary layer to the surface. A similar phenomenon has been observed in the context of rotor-stator interaction in an axial compressor [1].

In conclusion, the results from our 2D-CFD calculations suggest that the tower shadow does result in a noticeable unsteady component of the torque on the turbine shaft, and thereby on the power output as seen in the 3p effect of three-bladed turbines, even if they are upwind turbines. This result is consistent with an analysis by Dolan and Lehn [3]. A new result is the observation that a rather small overhang between tower and rotor may actually provide a mechanism to recover lift after entering stall conditions during part of the rotor's rotation, thus limiting the phenomenon of dynamic stall.

References

[1] A. Griebel and J. Seume. The influence of variable rotor-stator interaction on boundary-layer development in an axial compressor. In *Proceedings of GT2005: ASME Turbo Expo 2005: Power for Land, Sea and Air*, number GT2005-68902, Reno-Tahoe, Nevada, USA, 6 June 2005. ASME.

[2] A. Sathe and W. Bierbooms. Influence of different wind profiles due to varying atmospheric stability on the fatigue life of wind turbines. *J. Phys.: Conf. Ser.*, 75(1):012056, 2007.

[3] D.S.L. Dolan and P.W. Lehn. Simulation Model of Wind Turbine 3p Torque Oscillations due to Wind Shear and Tower Shadow. *IEEE Transactions on Energy Conversion*, 21(3):717–724, 2006.

[4] J.W. Larsen and S.R.K. Nielsen and S. Krenk. Dynamic stall model for wind turbine aerofoils. *Journal of Fluids and Structures*, 23(7):959 – 982, 2007.

[5] J. G. Leishman. Challenges in modelling the unsteady aerodynamics of wind turbines. *Wind Energy*, 5:85–132, 2002.

[6] N.M. Zoumakis and A.G. Kelessis. Methodology for bulk approximation of the wind profile power-law exponent under stable stratification. *Boundary-Layer Meteorology*, 55(1-2):199 – 203, 1990.

[7] S. Schreck. The NREL full-scale wind tunnel experiment. introduction to the special issue. *Wind Energy*, 5:77–84, 2002.

[8] D. Simms, S. Schreck, M. Hand, and L. J. Fingers. NREL unsteady aerodynamics experiment in the NASA-ames wind tunnel: A comparison of predictions to measurements. Technical Report Technical Report NREL/TP-500-29494, National Renewable Energy Laboratory, 2001.

[9] T. Thiringer and J.A. Dahlberg. Periodic pulsations from a three-bladed wind turbine. *IEEE Transactions on Energy Conversion*, 16(2):128 – 133, 2001.